ISSN 1063-7788, Physics of Atomic Nuclei, 2010, Vol. 73, No. 3, pp. 404–411. © Pleiades Publishing, Ltd., 2010.

NUCLEI
Theory

Elastic Scattering of Heavy Nuclei and Nucleus–Nucleus Potential with Repulsive Core*

V. Yu. Denisov and O. I. Davidovskaya

Institute for Nuclear Research, National Academy of Sciences of Ukraine, Kiev

Received March 25, 2009; in final form, August 6, 2009

Abstract—The elastic scattering of $^{16}O + ^{12}C$ at various collision energies is discussed in the framework of the optical model with repulsive core nucleus–nucleus potential. The cross sections on backward angles are strongly raised due to repulsive core. It is shown by using the near-side/far-side decomposition method that the near-side component of the scattering amplitude mainly contributes to the elastic scattering cross sections on forward and backward angles. The repulsive core of $^{16}O + ^{12}C$ potential takes place at distances $R \lesssim 3$ fm.

DOI: 10.1134/S1063778810030026

1. INTRODUCTION

The nucleus–nucleus interaction potential is a key ingredient in the analysis of nuclear reactions. By using the potential between nuclei we can evaluate the cross sections of different nuclear reactions [1–5].

The interaction potential between nuclei consists of nuclear, Coulomb, and centrifugal parts. The Coulomb and centrifugal interactions of two nuclei are well known. In contrast to this the nuclear part of nucleus–nucleus interaction is known worse. There are various approximations for the nuclear part of the nucleus–nucleus interaction potential.

The nuclear part of the interaction potential is often parameterized by the Woods–Saxon, the squared Woods–Saxon, or similar shapes [1–7]. This is phenomenological approach to the potential, which is very common. The parameters of the phenomenological potential are obtained by fitting the experimental data for various reactions. Therefore parameters of such potential depend on the reaction channel(s) and the model applied for reaction description.

There are several macroscopic, semi-microscopic and microscopic approaches for evaluation of the nucleus–nucleus potential [4, 5]. The proximity potential is derived in the framework of macroscopic approximation using the properties of nuclear matter, nuclear surface, density distributions in nuclei, and simple nucleon–nucleon interaction [8]. There are various semi-microscopic and microscopic models of nucleus–nucleus potential based on the Skyrme nucleon–nucleon forces [9–16] or simplified energy-density functional [16, 17]. Note that various properties of nuclear matter and nuclei are well described in the framework of the Hartree–Fock or the energy-density functional theories with effective Skyrme forces. The microscopic double-folding nucleus–nucleus potential is based on the M3Y, Paris, or Reid nucleon–nucleon forces and nucleon densities of the both nuclei [4, 5, 18–28]. The microscopic single-folding nucleus–nucleus potential is also used for description of heavy-ion reactions [1, 4, 5, 29].

The Woods–Saxon type, single- and double-folding [4, 5, 18–22, 24] potentials steadily rise from large negative value at $R = 0$ with increasing the distance R between nuclei. The nuclear part of these potentials is attractive at any distances between nuclei. In contrast to this the proximity potential [8], the potentials based on the Skyrme [9–13, 15], the modified M3Y [25–27], and the Reid soft-core [28] effective nucleon–nucleon forces are attractive at large and close distances between interacting nuclei and repulsive at very small distances, when colliding nuclei are strongly overlapped. The potentials based on the simplified energy-density functional [16, 17] have also repulsive core at small distances. In other words, there is repulsive core at small distances and attraction at larger distances for the proximity, the Skyrme-type, the modified M3Y, and the Reid soft-core potentials [8–13, 15–17, 25–27].

The nucleus–nucleus potential with repulsive core was discussed in [17] for the first time. The repulsion of two colliding nuclei at small distances, when densities of two nuclei are well overlapped and doubled in some volume, originated from the repulsion nature of nucleon–nucleon interaction at small distances due to 3-body-force contribution and the kinetic energy contribution due to the Pauli rearrangement and the

*The text was submitted by the authors in English.

antisymmetrization [9, 11, 17, 28]. Both the 3-body-force and the kinetic energy contributions into the nucleus–nucleus potential are directly taken into account in the framework of semi-microscopical models based on the Skyrme effective energy-density functional [9–13, 15].

Obvious example of the nature of repulsive core of the nucleus–nucleus potential is the potential evaluated in frozen nucleon densities for fully overlapped colliding nuclei, when the distance between nucleus–nucleus mass centers R is zero. In this case the density in inner part of overlapped nuclei is approximately twice higher than the normal density of nuclear matter. Such high-density state of nuclear matter is unstable, therefore local or absolute minimum of potential at $R = 0$ cannot exist. Therefore the result of potential evaluation based on the Skyrme force and frozen nucleon densities leading to the core at $R = 0$ is expected and natural. In contrast to this the microscopic double-folding nucleus–nucleus potentials based on the M3Y, Paris, or Reid nucleon–nucleon forces and frozen nucleon densities have the absolute minimum of potentials at $R = 0$ [4, 18–22, 24]. The origin of such very deep minimum is doubtful. Moreover, accounting of the nuclear three-body force leads to significant reduction of the depth of double-folding nucleus–nucleus potential [30].

The most part of experimental data for various nucleus–nucleus reactions have been analyzed using the Woods–Saxon type and double-folding potentials [1–7, 18–24]. However, only few reactions and potential properties have been considered applying the potentials with core [9–15, 17, 25–28, 31]. Therefore it is very interesting to analyze various reactions employing the potential with repulsive core.

The repulsion of colliding nuclei takes place at small distances between them. Therefore the influence of the repulsive core on reaction properties can appeare in reactions, which are very sensitive to values of the potential at small distances. Reaction of elastic scattering involved very stiff nuclei ^{16}O and ^{12}C at energies strongly above barrier is reasonable choice. This reaction is very sensitive to the potential values at small distances [21, 22, 24].

The $^{16}\mathrm{O} + {}^{12}\mathrm{C}$ elastic scattering data at several energies strongly above the barrier are measured by Ogloblin et al. [21, 22]. These data have been described by using very deep double-folding and Woods–Saxon potentials in [21, 22]. A shallow potential evaluated from a single-folding method was obtained in [29] for these reaction data sets. The $^{16}\mathrm{O} + {}^{12}\mathrm{C}$ and $^{16}\mathrm{O} + {}^{16}\mathrm{O}$ elastic scattering data are analyzed by using parabolic ℓ-dependent core recently [31]. However the nucleus–nucleus potential used in [31] is attractive at the core distances. Therefore it is very interesting to describe this reaction data using the repulsive core potential, which type is very similar to the Skyrme semi-microscopic potential.

In Section 2 of the paper we briefly discuss the parametrization of the phenomenological interaction potential with repulsive core. The discussion of the results and conclusion are given in Section 3.

2. POTENTIAL PARAMETRIZATION

The real part of the nucleus–nucleus potential $v(R)$ consists of Coulomb $v_{\mathrm{C}}(R)$, nuclear $v_n(R)$ and centrifugal $v_\ell(R)$ parts, i.e.,

$$v(R) = v_{\mathrm{C}}(R) + v_n(R) + v_\ell(R). \tag{1}$$

We propose writing the parts of nucleus–nucleus potential in the form

$$v_{\mathrm{C}}(R) = \begin{cases} \dfrac{Z_1 Z_2 e^2}{R}, & \text{if} \quad R \geq R_{\mathrm{C}}, \\ \dfrac{Z_1 Z_2 e^2}{R_{\mathrm{C}}} \left[\dfrac{3}{2} - \dfrac{R^2}{2R_{\mathrm{C}}^2} \right], & \text{if} \quad R < R_{\mathrm{C}}, \end{cases} \tag{2}$$

$$v_n(R) \tag{3}$$

$$= \frac{-V_0}{1 + \exp[(R - r_0(A_1^{1/3} + A_2^{1/3}))/d_0]} + V_{\mathrm{core}}(R),$$

$$v_\ell(R) = \frac{\hbar^2 \ell(\ell+1)}{2M[A_1 A_2/(A_1 + A_2)]R^2}. \tag{4}$$

Here, $A_{1,2}$ and $Z_{1,2}$ are, respectively, the number of nucleons and the number of protons in corresponding nuclei; e is the charge of proton; M is the mass of nucleon; $R_{\mathrm{C}} = r_{\mathrm{C}}(A_1^{1/3} + A_2^{1/3})$; $V_{\mathrm{core}}(R)$ is the core potential and ℓ is the orbital momentum value.

Let us consider the formation of the core part of the nucleus–nucleus potential in the framework of semi-microscopical model based on the Skyrme effective energy-density functional [10–12]. We use the frozen densities of nucleons. The approximation of frozen densities is also used in the double-folding model [4, 18–22, 24]. The interaction energy between nuclei at the center-to-center distance R is obtained as [10–12]

$$V(R) = \int d\mathbf{r} \varepsilon[\rho_{1p}(\mathbf{r}) + \rho_{2p}(\mathbf{R}, \mathbf{r}), \tag{5}$$

$$\rho_{1n}(\mathbf{r}) + \rho_{2n}(\mathbf{R}, \mathbf{r})] - \int d\mathbf{r} \varepsilon[\rho_{1p}(\mathbf{r}), \rho_{1n}(\mathbf{r})]$$

$$- \int d\mathbf{r} \varepsilon[\rho_{2p}(\mathbf{r}), \rho_{2n}(\mathbf{r})],$$

where $\varepsilon[\rho_{ip}(\mathbf{r}), \rho_{in}(\mathbf{r})]$ is the Skyrme energy-density functional. The first term in Eq. (5) is the energy of

the interacting nuclei at finite distance R, while the other ones are the energies of the noninteracting nuclei. The Skyrme energy-density functional for infinite nuclear matter takes the form [32]

$$\varepsilon[\rho_p(\mathbf{r}),\rho_n(\mathbf{r})] = \frac{\hbar^2}{2m}\tau + \frac{t_0}{2}\left[\left(1+\frac{x_0}{2}\right)\rho^2 - \left(x_0-\frac{1}{2}\right)\left(\rho_p^2+\rho_n^2\right)\right] + \frac{t_3}{12}\rho^\alpha\left[\left(1+\frac{x_3}{2}\right)\rho^2 - \left(x_3-\frac{1}{2}\right)\left(\rho_p^2+\rho_n^2\right)\right] + \frac{1}{4}\left[t_1\left(1+\frac{x_1}{2}\right)+t_2\left(1+\frac{x_2}{2}\right)\right]\rho\tau + \frac{1}{4}\left[t_2\left(x_2+\frac{1}{2}\right)-t_1\left(x_1+\frac{1}{2}\right)\right](\rho_p\tau_p+\rho_n\tau_n), \quad (6)$$

where $\tau_{p(n)} = \frac{3}{5}(3\pi^2)^{2/3}\rho_{p(n)}^{5/3}$ is the proton (neutron) kinetic energy evaluated in the Thomas–Fermi approximation; ρ_p and ρ_n are, respectively, the proton and neutron densities; $\rho = \rho_p + \rho_n$; $\tau = \tau_p + \tau_n$; t_0, t_1, t_2, t_3, x_0, x_1, x_2, x_3 are the Skyrme force parameters.

We propose that nuclear part of nucleus–nucleus potential is well parametrized by Woods–Saxon potential at large distances for the sake of simplicity. When the approaching nuclei are well overlapped then a volume, where the nucleon density is approximately doubled, is formed. The core part of the nucleus–nucleus potential is related to the volume of doubled density. It is easy to evaluate the volume of doubled nucleon density $v(R,a)$ for the step density distribution of two identical nucleus with radius a at distances $0 \le R \le 2a$ between them

$$v(R,a) = \frac{4\pi a^3}{3} - \pi R a^2 + \frac{\pi R^3}{12}. \quad (7)$$

Note that $v(0,a) = 4\pi a^3/3$ is the maximal volume, which can be filled with doubled density, and $v(R \ge 2a, a) = 0$.

The contribution of doubled-density volume into nuclear part of the potential can be estimated using Eqs. (5)–(7) and substitutions $\rho_p = \rho_n = \frac{1}{2}\rho = \frac{1}{2}\rho_0$ and $\rho_p = \rho_n = \frac{1}{2}\rho = \rho_0$ in the cases of saturated and doubled densities. As a result, we evaluate the core part of the nucleus–nucleus potential

$$V_{\text{core}}^{\text{Skyrme}}(R) = \left(\varepsilon\left[\rho_0,\rho_0\right] - 2\varepsilon\left[\frac{\rho_0}{2},\frac{\rho_0}{2}\right]\right), \quad (8)$$
$$v(R,a) \equiv C_{\text{core}}^{\text{Skyrme}} v(R,a),$$

where ρ_0 is the saturation density of nuclear matter. Substituting the corresponding values of parameters for the Skyrme force parametrization SkM* [32] and taking into account that a is the radius of ^{12}C ($a = \left(\frac{3\cdot 12}{4\pi\rho_0}\right)^{1/3}$ [fm], $\rho_0 = 0.1603$ fm^{-3} for SkM* [32]) we find

$$\left(\varepsilon\left[\rho_0,\rho_0\right] - 2\varepsilon\left[\frac{\rho_0}{2},\frac{\rho_0}{2}\right]\right) = C_{\text{core}}^{\text{SkM}^\star} \approx 3.296 \text{ MeV/fm}^3$$

and

$$V_{\text{core}}^{\text{SkM}^\star}(R=0) \approx 3.294 \text{ MeV/fm}^3 \times 74.86 \text{ fm}^3 \approx 246.6 \text{ MeV}.$$

So the contribution of core part of nucleus–nucleus potential at $R = 0$ is significant.

As is pointed, the repulsive part of the nucleus–nucleus potential is related to the exceeding density over the saturation density in some volume. Due to high density, considerable repulsive contributions of the 3-body-force and the kinetic energy appeared. The 3-body nucleon–nucleon force leads to strong repulsion at small distances between nucleons or high densities of nucleons [32, 33]. The 3-body-force contribution of the Skyrme force is proportional to t_3 parameter and the value of this parameter is very high for the Skyrme force [32, 33], for example, $t_3 = 15595$ MeV fm$^{3\alpha+3}$ for SkM* [32]. The contribution of nucleon kinetic energy into nucleus–nucleus potential is related to the Pauli rearrangement and the antisymmetrization on nucleons, belonging to different colliding nuclei. We apply the Thomas–Fermi approximation for evaluation of the kinetic energy contribution into nucleus–nucleus potential. Note that the nucleon kinetic energy and 3-body-force contributions are very important for evaluation of the compressibility values of nuclear matter especially for high values of densities.

We use simplified approximations for the nucleon density distributions and the energy-density functional at the evaluation of the core contribution into the nucleus–nucleus potential in Eq. (8). Therefore we parametrize the core part of potential at calculation of elastic scattering in similar to Eq. (8) form

$$V_{\text{core}}(R) = C_{\text{core}} v(R,a)^\gamma, \quad (9)$$

where C_{core}, a, and γ are fitting parameters, which depend on the collision energy. The dependence of these parameters on collision energy originated from both the momentum dependence of Skyrme force [33] and the dependence of the nucleon kinetic energy contribution on the collision energy, see, for example, in [23]. This parametrization of the core potential is different from the one considered in our previous work [34].

The imaginary part of the nucleus–nucleus potential consists of volume and surface parts, i.e.

$$W(R) = -\frac{W_w}{1+\exp[(R - r_w(A_1^{1/3} + A_2^{1/3}))/d_w]} \quad (10)$$
$$- \frac{W_s \exp[(R - r_s(A_1^{1/3} + A_2^{1/3}))/d_s]}{d_s\{1+\exp[(R - r_s(A_1^{1/3} + A_2^{1/3}))/d_s]\}^2},$$

where W_w and W_s are the strengths of volume and surface parts; r_w and r_s are the radius parameters of volume and surface parts; d_w and d_s are the diffusenesses of volume and surface parts. Such representation of the imaginary potential is common for theory of nucleus–nucleus collisions [1, 4, 5].

If 13 parameters $V_0, r_0, d_0, C_{\rm core}, a, \gamma, R_{\rm C}, W_w, r_w, d_w, W_s, r_s$ and d_s are known, then we can describe the angular distribution of nuclear reaction in the framework of optical model. Former 7 and latter 6 parameters are related to the real and imaginary parts of the potential, correspondingly.

3. RESULTS AND DISCUSSIONS

3.1. Elastic Scattering

We find 13 parameters of the potential by fitting the data for the $^{16}O + ^{12}C$ elastic scattering. For each collision energy we search the parameter set, which leads to the least

$$\chi^2 = \frac{1}{N}\sum_{i=1}^{N}\frac{(\sigma_{\rm calc}(\theta_i) - \sigma_{\rm exp}(\theta_i))^2}{\delta\sigma_{\rm exp}(\theta_i)}.$$

Here, N is the number of experimental points; $\sigma_{\rm calc}(\theta_i)$ and $\sigma_{\rm exp}(\theta_i)$ are, respectively, the theoretical and experimental values of the cross section at angle θ_i, and $\delta\sigma_{\rm exp}(\theta_i)$ is the corresponding error. To increase the weight of the data points at large angles, which are especially sensitive to the strength and shape of the optical potential at small distances, we have assumed, as in [22], for all data points $\delta\sigma_{\rm exp}(\theta_i) = 0.1\sigma_{\rm exp}(\theta_i)$. The scattering data are known at ^{16}O beam energies 132 MeV [21, 22], 169, 200, 230, 260 MeV [22], and 181 MeV [35]. The evaluated sets of potential parameters are given in the table.

Figures 1*a*, 1*b*, 1*c*, 1*d*, 1*e*, and 1*f* show the data and the optical model fits obtained by the potentials with repulsive core for energies 132, 169, 181, 200, 230, and 260 MeV, respectively. The total nucleus–nucleus potentials (1)–(4), (9) for $\ell = 0$ with parameters from the table at various collision energies are shown in Fig. 2. The repulsive core potentials have the core and the well, see Fig. 2. Note that the bottom of the well is the lowest value of the potential.

For manifestation of repulsive core effect we show in Fig. 1 the results of coreless optical model calculation ($C_{\rm core} = 0$). The optical model calculations for coreless potential are presented by dashed curves in Fig. 1. We see in Fig. 1 that the cross section increases on backward angles due to reflection from inner core. In contrast to this the values of cross section at forward angles are very similar for the both types of potentials.

We present in Fig. 1 the results of coreless optical model calculation ($C_{\rm core} = 0$) with optimized imaginary potential. The parameters W_w, r_w, d_w, W_s, r_s, and d_s of imaginary optical potential are fitted for best description of the experimental data in this case. The corresponding values of imaginary potential parameters are given in parentheses in the table. We see that results with optimized imaginary part better agree with experimental data on medium and back angles, however, additional oscillations appear. It is necessary to stress that the values of diffuseness of optimized imaginary potential d_w or d_s are very small $\lesssim$0.2 fm, see the table. It is well known that the sharp variation of optical potential leads to reflection [36]. So the reflection induced by sharp variation of imaginary potential for coreless potential with optimized imaginary part simulates the reflection from inner core of real part of optical potential with more smooth imaginary part. As a result, the cross sections on backward angles strongly increase in comparison to the results obtained for coreless potential without optimization of imaginary part. Note the origin of such sharp variation of imaginary part of optical potential is disputable.

Value of χ^2 evaluated with the repulsive core potential (see the table) for energy 132 MeV is lower than the one in [22] and higher than the one in [31]. (Note that our approach for evaluation of χ^2 values is the same as in [22] and different from the one in [31].) However, we obtain slightly larger values of χ^2 for other collision energies than the ones in [22, 31]. So, the quality of description obtained in our model is similar to the ones in [22, 31]. In contrast to this, the values of χ^2 presented in [29] are much larger than the corresponding ones in the table or in [22]. Note that the elastic $^{16}O + ^{12}C$ scattering data for beam energy 181 MeV have not been discussed in [21, 22, 29].

The forward angle cross sections evaluated using the strongly attractive nucleus–nucleus potentials show prominent the Fraunhofer diffraction structure with very deep and narrow dips, see figures in [21, 22]. The dips of the forward angle cross sections obtained in our approach are shallow, see Fig. 1.

The values of total reaction cross section presented in the table are close to the corresponding ones in [22]. The inner core has no effect on the total reaction cross-section values.

Sets of optical model parameters and related quantities used in analysis with repulsive core potential for the system $^{16}O + ^{12}C$. (The optimal parameters for imaginary part applied in optical model analysis with coreless potential are given in brackets)

E_{lab} [MeV]	132	169	181	200	230	260
V_0 [MeV]	19.593	21.558	21.531	21.871	21.857	22.004
r_0 [fm]	1.1831	1.0256	1.0796	1.0930	1.1633	1.1808
d_0 [fm]	0.6477	1.0059	0.9583	0.8624	0.6988	0.6428
C_{core} [MeV]	8.023	8.249	7.909	7.981	8.833	7.663
a [fm]	0.433	0.421	0.436	0.417	0.417	0.392
γ	1.151	1.030	0.996	0.997	0.882	0.891
r_c [fm]	1.268	1.198	1.261	1.255	1.357	1.158
W_w [MeV]	14.632	18.008	17.151	17.014	15.432	13.098
	(14.256)	(17.975)	(17.206)	(14.500)	(10.155)	(19.647)
r_w [fm]	1.156	1.008	1.058	1.057	1.111	1.081
	(1.320)	(0.985)	(1.216)	(0.984)	(1.220)	(1.072)
d_w [fm]	0.402	0.343	0.343	0.343	0.306	0.329
	(0.378)	(0.186)	(0.188)	(0.171)	(0.188)	(0.273)
W_s [MeV]	4.577	10.798	10.975	10.821	10.244	11.316
	(3.658)	(16.198)	(16.463)	(16.232)	(10.567)	(8.970)
r_s [fm]	1.362	1.240	1.273	1.266	1.300	1.276
	(1.168)	(1.198)	(1.242)	(1.202)	(1.290)	(1.364)
d_s [fm]	0.375	0.450	0.435	0.434	0.440	0.453
	(0.188)	(0.519)	(0.407)	(0.417)	(0.388)	(0.491)
J_R [MeV fm^3]	4.34	23.92	26.60	40.59	55.22	73.26
J_W [MeV fm^3]	70.68	72.62	78.91	77.72	79.69	70.12
σ [mb]*	1334.9	1368.9	1430.0	1391.5	1425.3	1421.9
χ^2	17.817	13.449	20.137	14.893	9.336	11.582

* The total reaction cross section.

3.2. Potentials

The repulsive core nucleus–nucleus potentials (1)–(4), (9) for $\ell = 0$ with parameters from the table at various collision energies are compared with the proximity [8] and semi-microscopic [10] potentials in Fig. 2.

The depth of pocket of the semi-microscopic potential is larger than the one of the phenomenological core-repulsion potentials for various collision energies. The depth of capture well depends slightly on the collision energy for the repulsive core potential, see Fig. 2. Different repulsive core potentials and the semi-microscopic potential are close to each other around barrier distances, while the proximity potential is too attractive at large distances between nuclei. The semi-microscopic potential and the repulsive core potentials obtained at various collision energies lead to very close values of the barrier heights. The positions of the capture well depths obtained for various collision energies take place at $R \approx 4$ fm. The

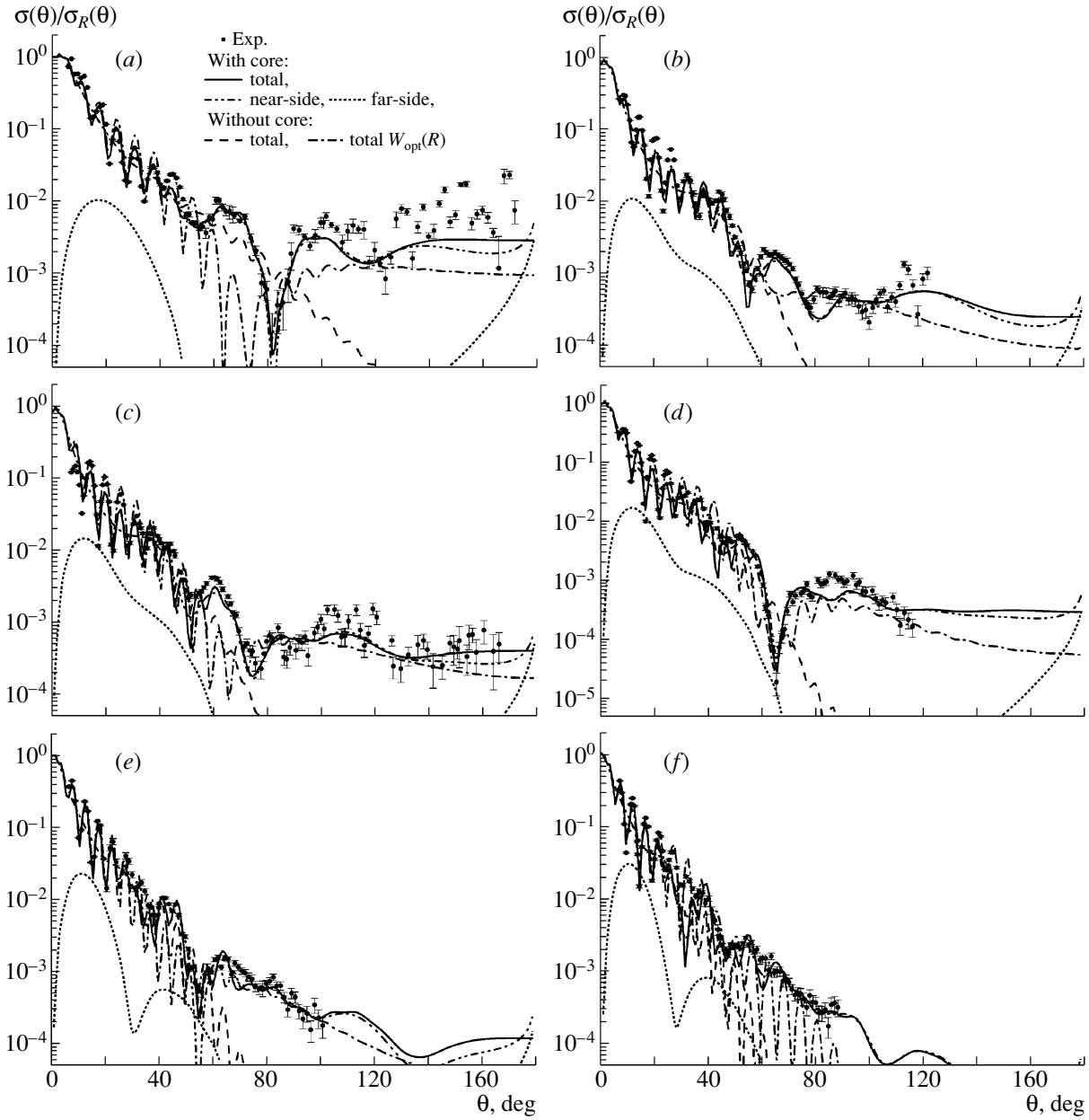

Fig. 1. Elastic-scattering data and the cross sections for total of the elastic $^{16}O + {}^{12}C$ scattering amplitude evaluated with (solid curve) and without (dashed curve) repulsive core in the potential at projectile ^{16}O energy 132 (*a*), 169 (*b*), 181 (*c*), 200 (*d*), 230 (*e*), 260 MeV (*f*). The cross sections for near-side (dash-dot-dotted curve) and far-side (dotted curve) decomposition of the elastic $^{16}O + {}^{12}C$ scattering amplitude evaluated with repulsive core in the potential. The cross sections for total of the elastic $^{16}O + {}^{12}C$ scattering amplitude with optimized imaginary potential (dash-dotted curve) are also presented.

repulsive core exits at distances $R \lesssim 3$ fm for potentials presented in Fig. 2. Therefore the distances, where the densities of colliding nuclei are well overlapped, and as a result, the 3-body force and kinetic energy contributions lead to strong repulsion, are similar for all potentials. The core radius evaluated by Gridnev et al. [31] is approximately 1.5–2 fm. Note that the core of nucleus–nucleus potential considered in [31] is ℓ-dependent. The shape of core proposed in [31] is different from the one described by Eq. (9).

The strong repulsion of potential appears at smaller distances, when the collision energy increases. The value of potential at $R = 0$ reduces with increasing of collision energy also.

The depths of the potentials evaluated in [22] for various energies belong to the range 170–362 MeV.

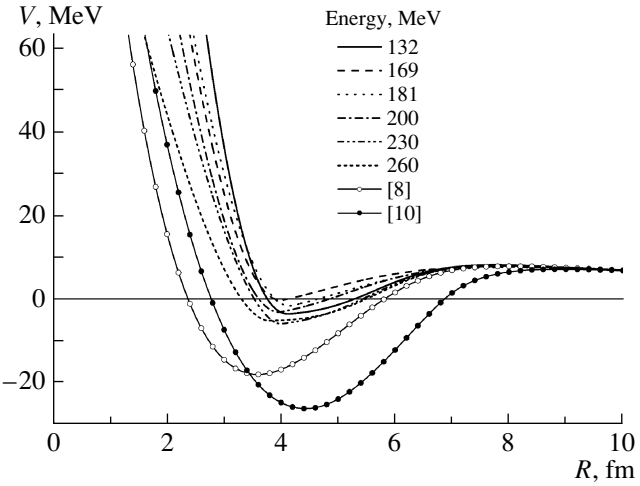

Fig. 2. The repulsive core potential evaluated for the elastic $^{16}O + {}^{12}C$ scattering for ^{16}O beam energies 132, 169, 181, 200, 230, and 260 MeV. The proximity [8] and semi-microscopic [10] potentials are also presented for reference.

Therefore the phenomenological repulsive core potentials (see Fig. 2) are shallower than the potentials obtained in [22]. The incorporation of the Pauli principle into the double-folding potentials based on the effective in-medium nucleon–nucleon interaction slightly reduces the depth of the double-folding potential [23, 28]. So, the potentials evaluated by using the Skyrme energy-density functional and various modified M3Y density-dependent nucleon–nucleon forces are very different at small distances.

The lowest values of the nuclear system formed in nucleus–nucleus collision at $R = 0$ is the energy of nucleus formed in fusion of these nuclei at the ground state $E_{\rm fus}$. Using Eq. (5) we find that the minimal value of the potential between nuclei at $R = 0$ is

$$V(R=0) \geq E_{\rm fus} - E_1 - E_2 \qquad (11)$$
$$= V_{\rm min}(R=0) = -Q_{\rm fus},$$

where E_i is the energy of nucleus i and $Q_{\rm fus}$ is the Q value of the nucleus–nucleus fusion reaction. Taking into account the experimental evaluation of the ground-state atomic masses [37] we obtain $V_{\rm min}(R = 0) = -16.75$ MeV for system $^{16}O + {}^{12}C$. Due to this, very deep attractive potential for this system at $R = 0$ is questionable as pointed in Introduction.

The volume integrals per interacting nucleon pair for real $J_V = -[4\pi/(A_1A_2)] \int v_n(R)R^2dR$ and imaginary $J_W = -[4\pi/(A_1A_2)] \int W(R)R^2dR$ parts of the potential are presented in the table. These quantities are often used as a sensitive measure of the potential strength. Our values of J_V are much smaller as compared with the corresponding ones in [22]. However, the values of J_W given in the table are close to the ones in [22]. So the strengths of imaginary potential are similar in both approaches and correspond to the regime of relatively weak absorption. Values of J_V and J_W increase with collision energy.

3.3. Near- and Far-Side Cross-Section Decomposition

The near-side/far-side decomposition technique [38] has proven to be of great help decomposing the interference caused by trajectories originating from different sides of the scattering potential. The convention states that trajectories being scattered into the same side from whence they came belong to the near-side, whereas trajectories scattered to the opposite side of the target are the far-side ones [38].

It is shown in [21, 22] by using Fuller's method that the $^{16}O + {}^{12}C$ elastic scattering cross section on forward angles is related to the near-side component, while the cross section for medium and back angles is determined by the far-side component. The far-side component is related to the rainbow phenomenon [24], which relates to the refraction of the incident wave by a strongly attractive (very deep) nucleus–nucleus potential. Many other interesting features connected to the near-side/far-side decomposition in the case of very deep nucleus–nucleus potential are discussed in [21, 22, 24].

We present the near-side/far-side decomposition of the elastic $^{16}O + {}^{12}C$ scattering amplitude in Fig. 1, which is evaluated using the repulsive core potentials. We see in Fig. 1 that the near-side component mainly describes the cross section in full range of angles. Contribution of the far-side component is noticeable on backwards angles. Due to the repulsive core the both near- and far-side components strongly rise on backward angles.

The repulsive core and coreless potentials are very shallow in comparison to the deep attractive nucleus–nucleus potentials from [21, 22, 24], therefore rainbow scattering is impossible in our case. However, we are able to describe scattering data by using the shallow potentials with repulsive core.

4. CONCLUSION

In conclusion, we show that:

(a) It is possible to describe elastic scattering data by using shallow phenomenological potential with the repulsive core.

(b) The elastic $^{16}O + ^{12}C$ scattering data shows that the repulsive core of nucleus–nucleus potential takes place at distances $R \lesssim 3$ fm.

(c) The cross section is mainly described by the near-side component of the scattering amplitude, when the phenomenological potential with the repulsive core is used.

(d) The cross section as well as both the near- and far-side cross-section components on backward angles are strongly enhanced by the repulsive core.

Similar results are obtained in our previous work [34], where another core potential parametrization is used.

ACKNOWLEDGMENTS

Authors thank a lot Dr. A.S. Dem'yanova for sending to us all the data for $^{16}O + ^{12}C$ elastic scattering used in this paper. Authors thank Profs. A.A. Ogloblin and W.H. Trzaska for their help in getting the data.

REFERENCES

1. P. E. Hodgson, *Nuclear Heavy-Ion Reactions* (Clarendon, Oxford, 1978).
2. R. Bass, *Nuclear Reactions with Heavy Ions* (Springer, Berlin, 1980).
3. W. Nörenberg and H. A. Weidenmüller, *Introduction to the Theory of Heavy-Ion Collisions* (Springer, Berlin, 1980).
4. G. R. Satchler, *Direct Nuclear Reactions* (Clarendon, Oxford, 1983).
5. P. Fröbrich and R. Lipperheide, *Theory of Nuclear Reactions* (Clarendon, Oxford, 1996).
6. A. Winther, Nucl. Phys. A **594**, 203 (1995).
7. K. Siwek-Wilczyńska and J. Wilczyński, Phys. Rev. C **69**, 024611 (2004).
8. J. Błocki, J. Randrup, W. J. Świateçki, and C. F. Tsang, Ann. Phys. (N.Y.) **105**, 427 (1977).
9. D. M. Brink and Fl. Stancu, Nucl. Phys. A **270**, 236 (1976); Fl. Stancu and D. M. Brink, Nucl. Phys. A **299**, 321 (1978).
10. V. Yu. Denisov, Phys. Lett. B **526**, 315 (2002).
11. V. Yu. Denisov and W. Nörenberg, Eur. Phys. J. A **15**, 375 (2002); V. Yu. Denisov, Eur. Phys. J. A **25** (Suppl. 1), 619 (2005).
12. V. Yu. Denisov and V. A. Nesterov, Phys. At. Nucl. **69**, 1472 (2006) [Yad. Fiz. **69**, 1507 (2006)].
13. V. Yu. Denisov and N. A. Pilipenko, Phys. Rev. C **76**, 014602 (2007).
14. J. Skalski, Acta Phys. Pol. B **34**, 1977 (2003); Int. J. Mod. Phys. E **13**, 305 (2004).
15. Min Liu, Ning Wang, Zhuxia Li, et al., Nucl. Phys. A **768**, 80 (2006).
16. C. Ngô, B. Tamain, J. Galin, et al., Nucl. Phys. A **240**, 353 (1975); H. Ngô and Ch. Ngô, Nucl. Phys. A **348**, 140 (1980).
17. K. A. Brueckner, J. R. Buchler, and M. M. Kelly, Phys. Rev. **173**, 944 (1968).
18. G. Bertsch, J. Borysowicz, H. McManus, and W. G. Love, Nucl. Phys. A **284**, 399 (1977); N. Anantaraman, H. Toki, and G. F. Bertsch, Nucl. Phys. A **398**, 269 (1983).
19. G. R. Satchler and W. G. Love, Phys. Rep. **55**, 183 (1979).
20. M. E. Brandan and G. R. Satchler, Phys. Rep. **285**, 143 (1997).
21. A. A. Ogloblin, Dao T. Khoa, Y. Kondō, et al., Phys. Rev. C **57**, 1797 (1998).
22. A. A. Ogloblin, Yu. A. Glukhov, W. H. Trzaska, et al., Phys. Rev. C **62**, 044601 (2000).
23. V. B. Soubbotin, W. von Oertzen, X. Viñas, et al., Phys. Rev. C **64**, 014601 (2001); K. A. Gridnev, V. B. Soubbotin, W. von Oertzen, et al., Phys. At. Nucl. **65**, 707 (2002)
24. Dao T. Khoa, W. von Oertzen, H. G. Bohlen, and S. Ohkubo, J. Phys. G **34**, R111 (2007).
25. E. Uegaki and Y. Abe, Prog. Theor. Phys. **90**, 615 (1993).
26. Ş. Mişicu and W. Greiner, Phys. Rev. C **69**, 054601 (2004).
27. Ş. Mişicu and H. Esbensen, Phys. Rev. Lett. **96**, 112701 (2006).
28. T. Izumoto, S. Krewald, and A. Faessler, Nucl. Phys. A **341**, 319 (1980); **357**, 487 (1981).
29. S. Hossain, M. N. A. Abdullah, K. M. Hasan, et al., Phys. Lett. B **636**, 248 (2006).
30. T. Furumoto, Y. Sakuragi, and Y. Yamamoto, Phys. Rev. C **79**, 011601 (2009).
31. K. A. Gridnev, E. E. Rodionova, and S. N. Fadeev, Phys. At. Nucl. **71**, 1262 (2008).
32. M. Brack, C. Guet, and H.-B. Håkansson, Phys. Rep. **123**, 275 (1985).
33. P. Ring and P. Schuck, *The Nuclear Many-Body Problem* (Springer, New York, 1980).
34. V. Yu. Denisov and O. I. Davidovskaya, in *Proc. of the 2nd Intern. Conf. on Current Problems in Nuclear Physics and Atomic Energy (NPAE-Kyiv 2008)* (Kyiv, Ukraine, 2009), p. 192.
35. A. S. Dem'yanova, private communication.
36. I. S. Shapiro, Usp. Fiz. Nauk **75**, 61 (1961) [Sov. Phys. Usp. **4**, 674 (1961)].
37. G. Audi, O. Bersillon, J. Blachot, and A. H. Wapstra, Nucl. Phys. A **729**, 3 (2003).
38. R. C. Fuller, Phys. Rev. C **12**, 1561 (1975).